Front. Phys. China, 2009, 4(2): 205–208
DOI 10.1007/s11467-009-0019-5

RESEARCH ARTICLE

Capacitive position measurement for high-precision space inertial sensor

Yan-zheng BAI (白彦峥), **Ze-bing ZHOU** (周泽兵) (✉), **Hai-bo TU** (涂海波), **Shu-chao WU** (吴书朝), **Lin CAI** (蔡林), **LI LIU** (刘力), **Jun LUO** (罗俊)

School of Physics, Huazhong University of Science and Technology, Wuhan 430074, China
E-mail: zhouzb@mail.hust.edu.cn

Received February 10, 2009; accepted March 2, 2009

Low noise position measurement is fundamental for space inertial sensors, and at present the capacitive position sensor is widely employed for space inertial sensors. The design for the possible suppression of the front-end electric noises for a capacitive sensor is presented. A prototype capacitive sensor with 2×10^{-6}pF/Hz$^{1/2}$ at frequency above 0.04 Hz is achieved and further improvements are discussed.

Keywords inertial sensor, accelerometer, capacitive position sensor

PACS numbers 04.80.-y, 06.30.Gv, 07.50.-e

1 Introduction

A high-precision space inertial sensor can usually work in two operation modes [1, 2]. One is the measurement of the non-gravitational forces of spacecraft (SC) as a force sensitive device, which is called the acceleration measurement mode here, such as the STAR and SuperSTAR accelerometers, with resolution of 3×10^{-9} m/(s^2·Hz$^{1/2}$) and 3×10^{-10} m/(s^2·Hz$^{1/2}$) at 0.1 Hz, respectively. These are employed in the Earth gravity satellites CHAMP and GRACE to measure the non-gravitational forces acting on the SC [3, 4]. Another is to guide the drag-free SC as a geodesic reference, which is called the inertia reference mode, such as the CAESAR, with an expected residual acceleration of 3×10^{-15}m/(s^2·Hz$^{1/2}$) at 0.1 mHz employed in the laser interferometer space antenna gravitational wave detection mission (LISA) [5, 6].

The operational principle of the space inertial sensor is schematically shown in Fig. 1. $a_{\rm s,g}$ and $a_{\rm p,g}$ are the gravitational accelerations acting on the SC and the proof mass (PM), respectively; $a_{\rm s,n}$ and $a_{\rm p,n}$ are the non-gravitational accelerations acting on the SC and the PM, respectively, which are induced by environment disturbances. $x = x_{\rm p} - x_{\rm s}$ is the relative displacement between the SC and the PM, while $x_{\rm n}$ is the position sensor noise. $a_{\rm s,fed}$ and $a_{\rm p,fed}$, respectively, are the equivalent feedback accelerations acting on the SC and the PM by the drag-free and electrostatic control loops. $H_{\rm t}$, $H_{\rm s}$, $H_{\rm a}$, $H_{\rm s,c}$ and $H_{\rm p,c}$ represent the transfer functions of the thruster, the position sensor, the electrostatic actuator, the drag-free controller, and the electrostatic force feedback controller, respectively. $\Gamma_{\rm n}$ is the thrust noise, and $V_{\rm n}$ is the feedback voltage noise of the electrostatic actuators. Ref. [7] presents a detailed analysis of the residual disturbance of the inertial sensor for the LISA mission.

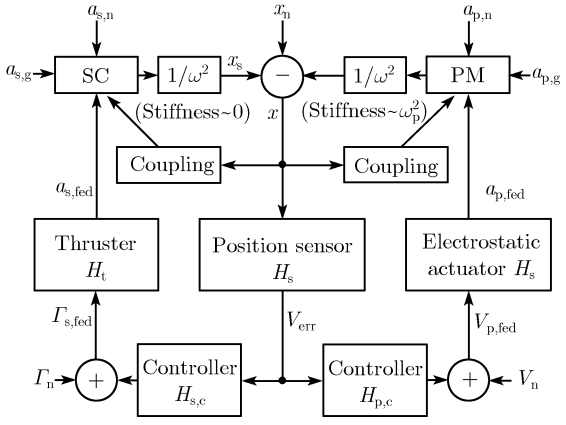

Fig. 1 Schematic diagram of the inertial sensors.

In the acceleration measurement mode, the closed-loop control will assure that the PM is servo controlled motionless in position and attitude with respect to the SC by the electrostatic actuators. Namely, the PM will always follow with the SC. In the measurement bandwidth, the residual acceleration disturbances of the PM

can be given by

$$a_{\mathrm{n,acc}} = a_{\mathrm{p,n}} + \omega_{\mathrm{p}}^2 x_{\mathrm{n}} + H_{\mathrm{a}} V_{\mathrm{n}} \tag{1}$$

where ω_{p}^2 is the parasitic stiffness coefficient per unit mass, which is induced by the position sensor and the position-dependent coupling action between the PM and the SC, such as the gravitation.

In the inertia reference mode, the non-gravitational forces acting on the SC such as the atmospheric drag, the solar and terrestrial radiation and so on will be compensated by the thrusters. In this case, the SC will follow with the PM and the residual acceleration disturbances of the PM can be given by [6, 7]

$$a_{\mathrm{n,df}} = a_{\mathrm{p,n}} + \omega_{\mathrm{p}}^2 (x_{\mathrm{n}} + x_{\mathrm{df,n}}) = a_{\mathrm{p,n}} + \omega_{\mathrm{p}}^2 \left(x_{\mathrm{n}} + \frac{\Gamma_{\mathrm{n}}}{H_{\mathrm{s}} H_{\mathrm{s,c}}} \right) \tag{2}$$

where $x_{\mathrm{df,n}}$ represents the control level of the SC by the drag-free control.

We can see that for both application modes of the space inertial sensors which form Eqs. (1) and (2), the key points for the space inertial sensor are to realize the low-noise position sensor, to reduce the coupling stiffness between the SC and the PM, to suppress or isolate the direction disturbances acting on the PM as much as possible, and to obtain high-performance control units and low-noise actuators or thrusters.

The many types of position sensors with a resolution at picometer level have been realized and tested in space missions, such as the capacitance transducer, the superconducting quantum interference devices (SQUID), the laser interferometer, and so on. The capacitive position sensor has been most widely applied in the high-precision space inertial sensor. In this paper, the design of a capacitive position sensor for the space inertial sensor is discussed and the progress in our laboratory is introduced.

2 Design and progress of capacitive position sensor

The capacitive position measurement can be realized by the gap-variation and area-variation configurations [8]. For the gap-variation configuration, we can easily obtain

$$\omega_{\mathrm{p}}^2 x_{\mathrm{n}} \propto C_{\mathrm{n}}/d_0 \tag{3}$$

where $\omega_{\mathrm{p}}^2 \propto C_0/d_0^2$ is the parasitic stiffness per unit mass induced by the capacitive sensor, $x_{\mathrm{n}} \propto C_{\mathrm{n}} d_0/C_0$ is the position noise limited by the capacitive measurement noise C_{n}, the electrode gap d_0 and the balance capacitance C_0. From Eq. (3), we can see that a high-precision capacitive sensor with a larger gap could reduce acceleration disturbance due to the back-action of the position sensor. However, the capacitive sensor with a larger gap will reduce the position measurement resolution and the acceleration measurement dynamic range, and also add the non-linear effect and edge-effect for the position measurement.

For the area-variation configuration, the parasitic stiffness $\omega_{\mathrm{p}}^2 \sim 0$ if we neglect the edge-effect and the cross couplings. However, the sensitivity of the area-variation capacitive sensor is limited, generally two orders smaller than that of the gap-variation in actual applications.

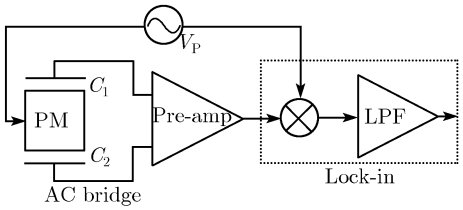

Fig. 2 Schematic diagram of capacitive sensor.

An ultra low noise capacitive sensor is very important for the inertial sensors. Capacitive sensors have been developed based on many kinds of methods, such as bridge-type measuring techniques [9, 10], frequency or phase shift method by resonance measuring techniques [11–13], charge transfer measuring principle [14], and so on. Low-noise technologies for capacitive sensors have also been investigated [15–18]. The capacitive sensor for the inertial sensor is usually based on the high sensitive AC-bridge and lock-in detection, which is shown in Fig. 2. The performance of the capacitive position sensor mainly depends on the front-end circuit of the capacitive sensor, namely the AC-bridge and the preamplifier. Figure 3 shows the typical electronics of the front-end circuit of the capacitive sensor. The AC-bridge consists of a differential transformer and the differential capacitances, wherein two electrodes sandwich the PM. A high-frequency driving voltage V_{p} is applied to the PM through a thin wire or an injection electrode, which aims to make the AC-bridge operate in high-frequency to reduce the low-frequency $1/f$ noises in electronic parts, and also to suppress the random noises by the demodulation. The unbalance signal is picked up by a charge amplifier and a lock-in amplifier. The performance of the capacitive sensor is determined by the non-ideal transformer and the noises of the preamplifier. The actual model of the three-winding transformer is shown in Fig. 3, where r is the series resistance, L is the shunt

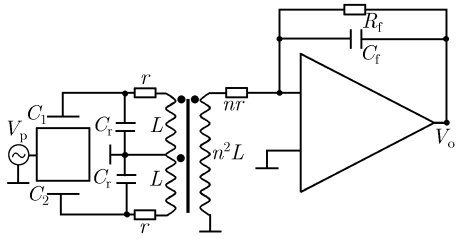

Fig. 3 Actual front-end electronics.

inductance, and n is the turn ratio between the secondary winding and primary winding [19].

The equivalent noise model of the front-end circuit is shown in Fig. 4. $e_{\rm n}$ and $i_{\rm n}$ respectively represent the equivalent input voltage and current noises of the operation amplifier. $e_{\rm f}$ and $e_{\rm s}$ respectively represent the thermal voltage noises of the source and feedback impedances $Z_{\rm s}$ and $Z_{\rm f}$. The source impedances can be obtained based on Fig. 3 as follows:

$$Z_{\rm s} = nr + \frac{1}{\dfrac{1}{n^2LS} + \dfrac{1}{n^2/\left(2C_{\rm t}S\right) + n^2r/2}} \tag{4}$$

where $C_{\rm t} = C_{\rm r} + C_0$, C_0 is the balancing capacitance, $C_{\rm r}$ is the parallel capacitance with the transformer, and S is the Laplace operator. The output voltage noise can be obtained as follows:

$$V_{\rm out,n} = \sqrt{\left|G\right|^2 e_{\rm s}^2 + e_{\rm f}^2 + \left|1+G\right|^2 e_{\rm n}^2 + \left|Z_{\rm f}\right|^2 i_{\rm n}^2} \tag{5}$$

where $G = Z_{\rm f}/Z_{\rm s}$, $Z_{\rm f} = R_{\rm f}/(1 + R_{\rm f}C_{\rm f}S)$. Due to large feedback impedance, the amplifier based on the Field Effect Transistor (FET) with the ultra-low current noise will be chosen preferably [8]. Due to the design noise level in the present IC electronics, the operation amplifier with $e_{\rm n}$ of nV/Hz$^{1/2}$ and $i_{\rm n}$ of fA/Hz$^{1/2}$ noise level is suitable for use. In this case, the effect by $i_{\rm n}$ is relatively weak and without consideration, however the input voltage noise $e_{\rm n}$ should be given more attention due to a gain enhancement of 1+G.

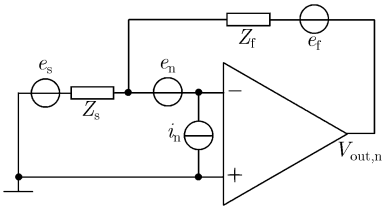

Fig. 4 Equivalent noise model of front-end electronics.

By neglecting the asymmetry and the leakage inductance of the differential transformer, the signal output is simply written as follows:

$$V_{\rm out,s} = -GHC_{\rm d}V_{\rm p} \approx -C_{\rm d}V_{\rm p}/(nC_{\rm f}) \tag{6}$$

where $C_{\rm d} = C_1 - C_2$, $H = nLS^2/(1 + C_{\rm t}rS + 2C_{\rm t}LS^2)$.

Compared with the Eqs. (5) and (6), we can see that the ratio $F = \left|\dfrac{GH}{1+G}\right| \approx \left|\dfrac{nLS^2}{1 + rC_{\rm t}S + 2LC_{\rm t}S^2}\right|$ should be large as soon as possible in order to suppress the effect of the $e_{\rm n}$. It is easy to obtain that the ratio F has a maximum at $1 + 2LC_{\rm t}S^2 = 0$ or $C_{\rm r} = 1/(2L\omega^2)$, as C_0 is relatively little. It means that an adequate capacitor $C_{\rm r}$ paralleling with the primary winding of the transformer can greatly improve the ratio F. The physical reason is that the capacitor $C_{\rm r}$ changes the source impedance to optimize the signal-to-noise ratio (SNR) with LC resonant. This was proven by comparing the output signal with and without the capacitor $C_{\rm r}$, as shown in Fig. 5. The solid line is the output voltage with the capacitor $C_{\rm r}$, and the noise level was reduced by about 15 dBm compared to that dashed line without the capacitor $C_{\rm r}$, while the peak at about 100 kHz pumping frequency serves as the signal related to the unbalanced input capacitances.

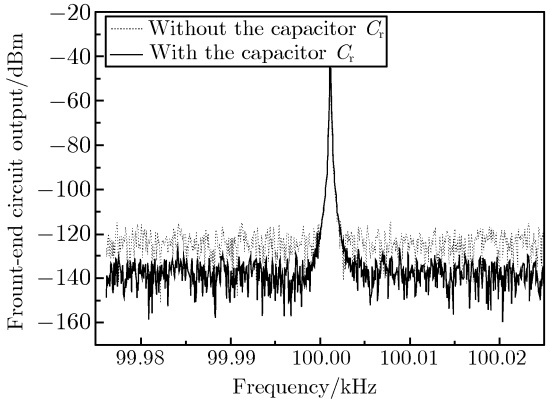

Fig. 5 Comparison result of ratio F with and without $C_{\rm r}$.

With the parallel capacitor $C_{\rm r}$, the power spectrum density (PSD) of the capacitive sensor was mainly limited by the voltage noises $e_{\rm s}$ and $e_{\rm f}$ as follows:

$$C_{\rm n} = \sqrt{\frac{2k_{\rm B}Tr}{L^2\omega^4V_{\rm P}^2} + \frac{4n^2k_{\rm B}T}{R_{\rm f}\omega^2V_{\rm P}^2}} \tag{7}$$

where ω is the angular frequency of the pumping signal $V_{\rm p}$, $k_{\rm B}$ is the Boltzmann constant, and T is the temperature. We can see that from the above equation, choosing the transformer with large L and small r can suppress the effect of $e_{\rm s}$, and choosing large feedback resistance $R_{\rm f}$ can suppress the effect of $e_{\rm f}$. It is notable that $R_{\rm f}$ is necessary to avoid DC saturation due to the input bias and offset currents of the amplifier. Choosing a low bias and offset input amplifier is useful for admitting a larger feedback transistor $R_{\rm f}$.

A prototype capacitive sensor with a sensitivity of 1.91 V/pF was achieved in our laboratory. The sensitivity was calibrated by a moved differential electrode compared with a capacitance-meter Agilent 4288 A with an accuracy of 0.07%. The noise PSD of the prototype capacitive sensor is plotted in Fig. 6. The resolution of the sensor came to about 2×10^{-6} pF/Hz$^{1/2}$ above 0.04 Hz, which is about one order higher than the theoretical estimation. The possible reasons are the inadequate design of system grounding and the noise limit of subsequent analog circuits. In addition, the effect of the phase noise of the pumping signal should be carefully considered. The corresponding displacement resolution for the capacitance with a gap of 150 μm and a surface area of 4 cm^2 is about 10 pm/Hz$^{1/2}$. The noises below 0.04 Hz are nearly inversed to frequency.

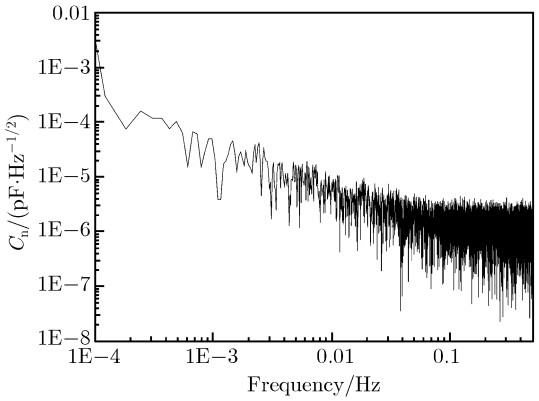

Fig. 6 The power spectrum noise of a prototype capacitive sensor.

3 Discussion

The design for a low-noise front-end capacitive sensor was discussed, and then a prototype capacitive sensor with 2×10^{-6} pF/Hz$^{1/2}$ above 0.04 Hz was developed for the capacitive inertial sensors. Problems with grounding, electromagnetic compatibility (EMC), and reducing the corner frequency of $1/f$ noise will be carefully investigated in future.

High-precision inertial sensors are one of keys of the Satellite Earth gravity field measurement and space gravitational experiments. The fundamental of the inertial sensor is to develop a low-noise position sensor and to investigate and suppress direct disturbances. There is a trade-off between the high sensitivity and the low back-action for the position sensor. The capacitive sensor based on the area-variation configuration [20] and all optical position sensors [5, 21] with much weaker coupling are good candidates for higher precision inertial sensors.

Acknowledgements This work was supported by the National Natural Science Foundation of China (Grant No. 10675047).

References

1. Y. Z. Bai, H. B. Tu, Z. B. Zhou, S. C. Wu, and J. Luo, J. Jpn. Soc. Microgravity Appl., 2008, 25: 423
2. P. Touboul, B. Foulon, and E. Willemenot, Acta Astronautica, 1999, 45(10): 605
3. M. Rodrigues, B. Foulon, F. Liorzou, and P. Touboul, Class. Quantum Grav., 2003, 20: S291
4. J. Flury, S. Bettadpur, and B. D. Tapley, Adv. Sp. Res., 2008, 42: 1414
5. LISA System and Technology Study Report, ESA–SCI 11, July 2000
6. S. Vitale, P. Bender, A. Brillet, S. Buchman, A. Cavalleri, M. Cerdonio, M. Cruise, C. Cutler, K. Danzmann, R. Dolesi, W. Folkner, A. Gianolio, Y. Jafry, Gunther. Hasinger, G. Heinzel, C. Hogan, M. Hueller, J. Hough, S. Phinney, T. Prince, D. Richstone, D. Robertson, M. Rodrigues, A. Rudiger, M. Sandford, R. Schilling, D. Shoemaker, B. Schutz, R. Stebbins, C. Stubbs, T. Sumner, K. Thorne, M. Tinto, P. Touboul, H. Ward, W. Weber, and W. Winkler, Nucl. Phys. B (Proc. Suppl.), 2002, 110: 209
7. B. L. Schumaker, Class. Quantum Grav., 2003, 20: S239
8. V. Josselin, P. Touboul, and R. Kielbasa, Sensors and Actuators A, 1999, 78: 92
9. O. Petersons, IEEE Trans. Instrum. Meas., 1964, 13(4): 216
10. K. Watanabe and G. C. Temes, IEEE Trans. Instrum. Meas., 1984, 33(4): 247
11. T. Kataoka and M. Kanno, Instrumentation and Measurement Technology Conference, May 10–12, 1994, 2: 1008
12. M. Bramanti, IEEE Trans. Ind. Electron., 1990, 37(6): 584
13. S. Natarajan and B. K. Herman, Twenty-Second Southeastern Symposium on System Theory, March 11–13, 1990: 46
14. S. M. Huang, R. G. Green, A. Plaskowski, and M. S. Beck, IEEE Trans. Instrum. Meas., 1988, 37(3): 368
15. X. L. Zhang and P. K. Chan, IEEE Trans. Instrum. Meas., 2008, 57(7): 1492
16. S. Adl and M. Peckerar, IEEE Sensors Applications Symposium, San Diego, February 6–8, 2007
17. M. Bingesser et al., Design Automation and Test in Europe, March 10–14, 2008: 868
18. Z. F. Wang, Z. H. Li, X. W. Ni, and B. X. Mo, 8$^{\mathrm{th}}$ International Conference on Solid-State and Integrated Circuit Technology, October 23–26, 2006: 673
19. W. H. P. Leslie, The Institution of Electrical Engineers, 1961, 3646: 539
20. J. Josselin, R. Chhun, P. Touboul, and G. Metris, 59th International Astronautical Congress, Glasgow, September 29–October 3, 2008
21. K. X. Sun, G. Allen, S. Buchman, D. Debra, and R. Byer, Class. Quantum Grav., 2005, 22: S287